Title
Optical probing of local membrane potential with fluorescent polystyrene beads

Journal
Biophysical Reports, 1(2)

ISSN
2667-0747

Authors
Shapira, Zehavit
Degani-Katzav, Nurit
Yudovich, Shimon
et al.

Publication Date
2021-12-01

DOI
10.1016/j.bpr.2021.100030

Peer reviewed

Biophysical Reports

REPORT

Optical probing of local membrane potential with fluorescent polystyrene beads

Zehavit Shapira,[1,2] Nurit Degani-Katzav,[1,2] Shimon Yudovich,[1,2] Asaf Grupi,[1,2] and Shimon Weiss[1,2,3,4,*]

[1]Department of Physics and [2]Institute for Nanotechnology and Advanced Materials, Bar-Ilan University, Ramat-Gan, Israel; and [3]Department of Chemistry and Biochemistry and [4]California NanoSystems Institute, University of California Los Angeles, Los Angeles, California

ABSTRACT The study of electrical activity in single cells and local circuits of excitable cells, such as neurons, requires an easy-to-use, high-throughput methodology that allows for the measurement of membrane potential. Investigating the electrical properties in specific subcompartments of neurons, or in a specific type of neurons, introduces additional complexity. An optical voltage-imaging technique that allows high spatial and temporal resolution could be an ideal solution. However, most valid voltage-imaging techniques are nonspecific. Those that are more site-directed require a lot of preliminary work and specific adaptations, among other drawbacks. Here, we explore a new method for membrane voltage imaging, based on Förster resonance energy transfer between fluorescent polystyrene (FPS) beads and dipicrylamine. Not only has it been shown that fluorescence intensity correlates with membrane potential, but more importantly, the membrane potential from individual particles can be detected. Among other advantages, FPS beads can be synthesized with surface functional groups and can be targeted to specific proteins by conjugation of recognition molecules. Therefore, in the presence of dipicrylamine, FPS beads represent single-particle detectors of membrane potential that can be localized to specific membrane compartments. This new and easily accessible platform for targeted optical voltage imaging can further elucidate the mechanisms of neuronal electrical activity.

WHY IT MATTERS We present a novel, to our knowledge, method for studying electrical signals at the nanoscale, down to the level of a single synapse—the structure that enables the transmission of signals from one neuron to another. This method relies on energy transfer between a fluorescent polystyrene bead and a negatively charged quencher molecule added to the membrane. Using specific antibodies, this nanoscale voltage sensor can be specifically targeted to the synapse and report its neuronal electrical activity.

INTRODUCTION

The study of the electrical properties of excitable cells, such as neurons and muscle cells, is a crucial study in neuroscience. The traditional method in electrophysiology for measuring membrane potential is the patch-clamp technique. This method allows high-resolution electrophysiological recordings from single cells down to single channels. It allows for measurements of membrane voltage changes in primary cultured neurons as well as in cultured cell lines. However, a major drawback of this method is the use of invasive electrodes that limit measurements to single cells and result in low-throughput screening assays. A different high-throughput assay is needed for electrical measurements from assembly of cells and from different parts of the single neuron itself, such as dendrites and spines. Optical techniques that correlate membrane potential with fluorescent response can compensate for these drawbacks. They are relatively noninvasive, provide spatial resolution in assemblies of cells or in subcellular regions, and are high throughput.

There are several optical imaging techniques used for the investigation of neuronal activity. One standard technology is calcium imaging (1), which enables the assessment of the network activity of neurons based on intracellular calcium concentration as an indicator of neural activity. Significant disadvantages of this method are the lack of information about hyperpolarizing and subthreshold depolarizing signals, low temporal resolution, and high background noise.

Voltage-sensitive dyes that allow direct fluorescence imaging of membrane voltage changes (in vitro and

Submitted April 26, 2021, and accepted for publication October 27, 2021.

*Correspondence: sweiss@chem.ucla.edu

Zehavit Shapira and Nurit Degani-Katzav contributed equally to this work.

Editor: Hagen Hofmann.

https://doi.org/10.1016/j.bpr.2021.100030

in vivo) (2,3) are successfully used for neuroimaging at the ensemble dye level in both in vitro and in vivo formats. However, their potential for neuroimaging is not fully exploited because of shortcomings such as alteration of membrane capacitance, phototoxicity, photobleaching, and nonspecific background labeling. More importantly, they only display nonspecific staining, and they do not allow for localized, nanoscale (subdiffraction limit) site-specific membrane potential measurements.

Genetically encoded voltage indicators (GEVIs) have been developed to measure voltage signals from small neurons and subcellular regions (4). Yet, detection of action potentials (APs) is limited because many suffer from relatively low sensitivity (5), poor expression (6), and relatively slow kinetics (5,7,8). A new generation of improved GEVIs has allowed for simultaneous recordings from multiple neurons in behaving animals, with good temporal response (9–11).

Hybrid approaches combining chemically synthesized dyes with genetically introduced proteins have also been developed, such as the rhodamine-based voltage reporters, which can be covalently linked to genetically introduced enzymes. Rhodamine-based voltage receptors have been used to record APs in single trials, together with the green fluorescent Ca^{2+} indicator GCaMP for simultaneous voltage and Ca^{2+} recordings (2). Another example is the new VoltageSpy dyes that target the genetically introduced cell-surface SpyCatcher with fast temporal response (12). These new developments provide faster temporal resolution (compared with Ca^{2+} imaging) and diffraction-limited spatial resolution (compared with low spatial resolution of traditional electrode-based recordings).

Recently, voltage-sensing nanoparticles (vsNPs), such as voltage-sensing quantum dots (13), have been developed for noninvasive optical recording of membrane potential at the single-particle and nanoscale levels, at multiple locations, and in a large field-of-view. In contrast to voltage-sensitive dyes and GEVIs, vsNPs allow for "pointy," single-particle voltage detection. However, vsNPs still face challenges associated with functionalization, bioconjugation, stable membrane insertion, toxicity, and uniformity (14–18). Additional improvements are needed before this new generation of sensors can be widely translated to neurophysiological applications.

Another interesting mechanism of optical voltage sensors is based on Förster resonance energy transfer (FRET) between membrane-embedded fluorescent donors and translocating oxonol acceptors (19). Dioctadecyloxacarbocyanine (DiO)/dipicrylamine (DPA) is a well-known FRET-based membrane potential detection system. DiO is a nontoxic fluorescent lipophilic dye that readily labels membranes. It serves as a stationery FRET donor in the plasma membrane. DPA serves as a mobile FRET acceptor. DPA is a nonfluorescent lipophilic anion that distributes between leaflets of the lipid bilayer in response to membrane potential, thus acting as a voltage sensor.

Our aim was to use this mechanism to develop a single-particle voltage detection system that would allow membrane potential measurements in localized nanoscale areas with subdiffraction resolution. The significance of measuring subdiffraction local membrane potential is documented in (20), in which the authors were able to record the electrical signal from individual spines with a nanopipette and come up with an equivalent electrical circuit for the spine. Similarly, recording electrical signals from pre- and postsynaptic membranes (of the same synapse) would require subdiffraction recording and would provide a wealth of new information.

To achieve this goal, nanoparticles were considered to be used as the stationery FRET donors instead of DiO. Fluorescent polystyrene (FPS) beads were identified as the potential candidates. These beads are commercially available in a range of uniform sizes (down to ~20 nm in diameter) and can be loaded with dyes spectrally suitable for FRET interaction with DPA.

The potential for FPS beads to act as vsNPs is also attributed to the fact that FPS beads typically have a very thin layer of surface groups, which brings the surface of the FPS beads to practically direct contact with the plasma membrane. Because the fluorophores encapsulated within the FPS bead are homogenously distributed, the population of fluorophores closest to the membrane surface may FRET with DPA distributed in the plasma membrane.

Therefore, FPS beads with an emission spectral that overlaps with the absorbance of DPA were selected (Fig. 1 *A*). The essence of the mechanism is as follows: the beads are applied to the bath solution and attach the cell membrane from the outside, and the negatively charged DPA molecules in the membrane redistribute in response to the membrane potential. At negative potentials, the DPA molecules move closer to the outer leaflet of the membrane, resulting in quenching of the bead's fluorophores. Conversely, upon depolarization, the DPA molecules move away from the beads toward the inner leaflet, so the fluorophores are unquenched (Fig. 1 *B*).

In this work, the potential of FPS beads (with a hydrodynamic diameter of ~70 nm) as voltage nanosensors is explored. The performance of these beads as the donor particles to DPA is determined in HEK293 cells and primary cortical neurons. Fluorescence response to membrane potential changes is demonstrated from ensemble membrane staining as well as from single spots. In conclusion, this system's sensitivity is adequate to perform membrane potential imaging

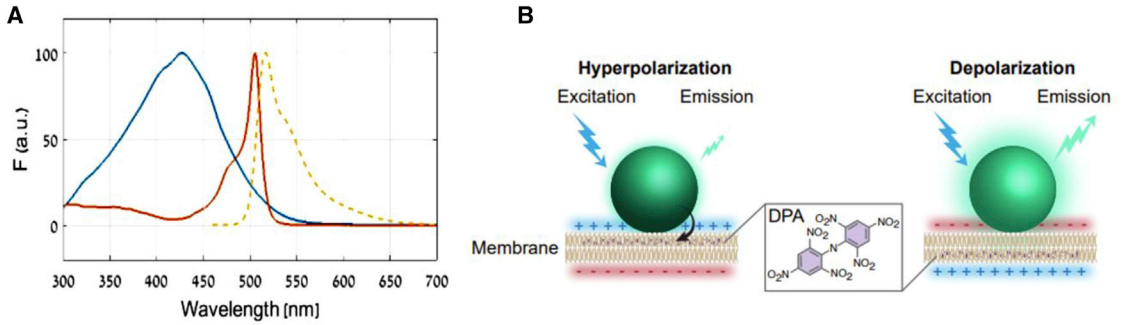

FIGURE 1 The FPS beads/DPA FRET pair mechanism. (*A*) Absorption spectrum of DPA (*blue*) and absorption (*orange*) and fluorescence emission (*dashed yellow*) spectra of FPS beads. An overlap of the FPS beads emission and DPA absorption enables FRET between the two species. (*B*) The FPS beads are attached to the extracellular side of the cell membrane; at hyperpolarization, DPA molecules translocate to the outer leaflet of the membrane and closer to the beads, resulting in FRET and a decrease in the bead's fluorescence. Upon depolarization, the DPA molecules redistribute to the inner leaflet and away from the beads, resulting in an increase of the bead's fluorescence.

from single particles, whereas from the aspect of kinetics, the temporal response is currently limited to ~5 ms.

MATERIALS AND METHODS

Cell line culture preparation

Human embryonic kidney (HEK293) cells were cultured in Dulbecco's modified eagle medium containing 10% fetal calf serum, 2 mM glutamine, 100 units/mL penicillin G, and 100 μg/mL streptomycin and grown in 5% CO_2 at 37°C under 90–95% humidity. For electrophysiology experiments, the cells were seeded on glass coverslips (25 mm diameter) placed in six-well plates and precoated with poly-D-lysine. Electrophysiology experiments were performed 24–48 h after seeding with a cell confluence of 70%.

Cortical neuron culture preparation

All animal experiments were approved by the local ethics committee for animal research (ethical approval number 63-09-2018). Primary cortical neurons were cultured from P1 and P2 newborn Sprague Dawley rats. The tissue was digested by 100 units of papain (Sigma-Aldrich, St. Louis, MO) in Ca^{2+}/Mg^{2+}-free Hank's balanced salt solution (Biological Industries, Beit HaEmek, Israel) for 20 min in a 37°C incubator. The tissue was then mechanically dissociated, and the cells were plated on 50 μg/mL poly-D-lysine-coated coverglasses in Neurobasal medium (Biological Industries) supplemented with 2% B-27 (Invitrogen, Waltham, MA), GlutaMAX-I 2 mM (Invitrogen), penicillin (100 unit/mL)/streptomycin (100 μg/mL) (Biological Industries), 5.5 μM glucose, and 5% normal horse serum (Biological Industries). On the following day and twice a week thereafter, the medium was exchanged with growth medium, containing the same components as described above, with the neurobasal medium exchanged with minimal essential media. Once a week, the medium was applied with 5 μM Ara-C to prevent glial proliferation. Cells were incubated at 37°C in a humidified 5% CO_2 incubator. The experiments were conducted at 10–15 days *in-vitro* (DIV).

Staining cells with FPS beads and DPA

For HEK cells loading, 0.06 μm carboxyl FPS yellow beads (Spherotech, Lake Forest, IL) were briefly sonicated and diluted right before use in Dulbecco's phosphate buffered saline to final concentrations of 500 pM for ensemble staining and for 5 or 1 pM for single spots staining. DPA (20 mM in DMSO; Biotium, Fremont, CA) was diluted right before use in HEK external solution (detailed below). HEK cells seeded on glass coverslips were incubated with FPS beads for 10 min at room temperature, washed, applied with DPA, and immediately taken for imaging. For neurons loading, the particles were sonicated and diluted to final concentrations of 22 pM in neuronal external solution (detailed below). The cells were incubated for 5 min in room temperature, washed, and applied with fresh DPA diluted in neuronal external solution.

Electrophysiological recording

Voltage-clamp recordings in HEK cells were performed using the whole-cell configuration of the patch-clamp technique. The recordings were performed using a computer-controlled amplifier (EPC 10 USB, HEKA Elektronik, Reutlingen, Germany). Recorded signals were filtered at 10 kHz using a Bessel filter and digitized at 10–100 kHz, depending on the timescale of the voltage waveform.

The imaging and electrophysiology experiments using HEK cells were conducted with the HEK external solution containing (in mM) the following: 140 NaCl, 2.8 KCl, 2 $CaCl_2$, 1 $MgCl_2$, 10 HEPES, and 10 glucose, adjusted with NaOH to pH 7.4 (310 mOsm). The pipette solution contained (in mM) the following: 125 K-gluconate, 0.6 $MgCl_2$, 0.1 $CaCl_2$, 1 EGTA, 10 HEPES, 4 Mg-ATP, and 0.4 Na_2GTP, adjusted with KOH to pH 7.4 (295 mOsm). For experiments conducted in neurons, the neuronal external solution contained (in mM) the following: 116.9 NaCl, 2.7 KCl, 1.8 $CaCl_2$, 0.5 $MgCl_2$, 20 HEPES, 5.5 glucose, 0.36 NaH_2PO_4, 200 ascorbic acid, penicillin (100 unit/mL final), and streptomycin (100 μg/mL final) at pH 7.3 and adjusted to 320 mOsm with sucrose. The neuronal pipette solution contained (in mM) the following: 110 K-gluconate, 10 KCl, 10 glucose, 8 sodium creatine-phosphate, 5 EGTA, 10 HEPES, 4 Mg-ATP, and 0.4 Na-GTP (pH 7.3), adjusted to 290 mOsm with sucrose. The patch pipettes were pulled from borosilicate glass (Warner Instruments, Hamden, CT) with a resistance of 5–10 MΩ when filled with the pipette solution.

Optical recordings

Imaging was performed using a light-emitting diode excitation (SPECTRA X; Lumencor, Beaverton, OR) passing through a 470/24 nm bandpass filter and an electon-multiplying charge-coupled device camera (iXon Ultra 897; Andor, Belfast, UK), coupled to a motorized inverted microscope (IX83; Olympus, Tokyo, Japan). All imaging was performed using a 100× oil-immersion objective (UAPON100XOTIRF; Olympus), apart from the data shown in Fig. 3, in which a 60×

oil-immersion objective (UPLSAPO60XO; Olympus) was used. Fluorescence emission was filtered with a bandpass filter (ET520/20m; Chroma Technology, Bellows Falls, VT). A data acquisition device (USB-6211; National Instruments, Austin, TX), controlled by a home-written software (LabVIEW; National Instruments), was used for synchronizing the camera and the patch-clamp amplifier.

Data analysis

Analysis of fluorescence imaging of clamped cells was performed in MATLAB (The MathWorks, Natick, MA). For sparse staining, a two-dimensional particle tracking algorithm was used to correct for small translations, mainly because of mechanical drift and cellular motion exerted by the patch pipette. Fluorescence intensity for each frame was calculated by averaging the 10 brightest pixels of each spot for sparse staining and averaging the fluorescence from the whole cell for ensemble measurements. For the latter, background subtraction of each frame was performed by subtracting the mean value of the 10% darkest pixels. Fluorescence trajectories were corrected for photobleaching by either a high-pass filter or subtraction of the fluorescence trajectory by a two-term exponential function fitted to the baseline voltage levels. The average optical voltage response for each intensity trajectory was calculated by averaging the intensity value corresponding to every voltage level. To achieve a stabilized value of the response, the averaging was performed on the frame containing the last 100 ms of each voltage step.

Data and code depository

Raw data fluorescent images of all voltage and electrical measurements for this paper can be found at (https://zenodo.org, https://zenodo.org/record/4701597#.YYYXSJ5ByUl). Home-written code (MATLAB) for extraction and analysis of recorded electrophysiological optical trajectories is available upon request.

RESULTS

FPS beads and DPA comprise a membrane potential detector because of FRET reactions

As was detailed above, the FRET pair combined from DiO, a membrane dye, and DPA was described as a successful optical reporter for membrane potential (21). To test the fluorescence response of the FPS beads/DPA FRET pair to changes in membrane potential (Fig. 1 *B*), simultaneous optical and electrical recordings were conducted. Isolated HEK293 cells were labeled with beads, followed by a replacement of the bath solution to an external recording solution containing DPA (see Materials and methods). Using the whole-cell configuration of the patch-clamp technique, voltage steps were applied to the cell membrane. During the voltage protocol activation, the cells were excited with 485 nm, and the fluorescence intensity was monitored (Fig. 2). When using the 60 mV steps voltage protocol described in Fig. 2 *C*, the fluorescence intensity increased upon depolarization with an averaged relative change $\Delta F/F$ of 5.6 $\pm$ 2.4% per 120 mV (n $=$ 11) in the presence of 2 μM DPA in the bath solution. The labeling was stable after 2 h in the bath solution, and patch-clamp experiments were still successfully applicable. The fluorescence increased as the membrane potential increased, in accordance with the beads/DPA FRET mechanism described before. As the membrane potential increases, the DPA molecules tend to be closer to the inner leaflet of the membrane, resulting in unquenching of the beads fluorescence.

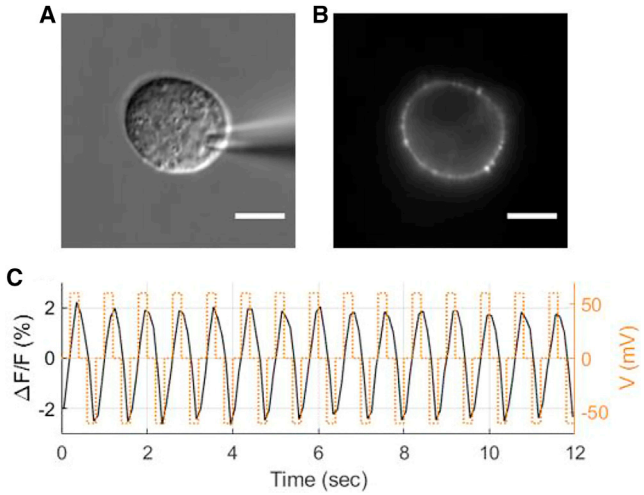

FIGURE 2 The fluorescence response of FPS beads/DPA FRET pair to membrane voltage in HEK cells. A differential interference contrast (DIC) (*A*) and a fluorescence (*B*) image of a single HEK cell in the whole-cell patch-clamp mode, labeled with 0.5 nM beads, in the presence of 2 μM DPA in the bath solution. The patch electrode is seen in (*A*). The cells were clamped to a square voltage waveform consisting of 0, 60, 0, and $-$60 mV voltage levels, each 200 ms in duration. (*C*) shows the fluorescence response (*black*, *solid*) upon changes in membrane potential (*orange*, *dashed*). The average change in fluorescence emission ΔF/F from the cell was 4.3 $\pm$ 0.2% per 120 mV. Scale bars, 10 μm.

The fluorescence response of FPS beads/DPA was further investigated. The fluorescence response as a function of membrane potential was tested for different DPA concentrations, ranging from 0.5 to 5 μM (Fig. 3; Fig. S1). As expected, the relative change in fluorescence intensity $\Delta F/F$ increased in the presence of higher concentrations of DPA in the bath solution because a higher concentration of DPA leads to more quenching of the beads fluorescence. Moreover, as shown in Fig. 3 *B*, the ΔF/F for highly positive membrane potentials increased as the DPA concentration increased, whereas it reached a steady state at lower DPA concentrations. The averaged $\Delta F/F$ at a membrane potential of $+$80 mV relative to the holding potential of $-$60 mV was 2.09 $\pm$ 0.34 and 5.62 $\pm$ 1.28% at 0.5 and 5 μM DPA, respectively (Fig. 3 *B*). The averaged $\Delta F/F$ at $+$60 mV and $-$60 mV relative to 0 mV in different DPA concentrations is also shown in Fig. S1. Control experiments were also conducted in HEK cells to confirm there is no significant response derived from

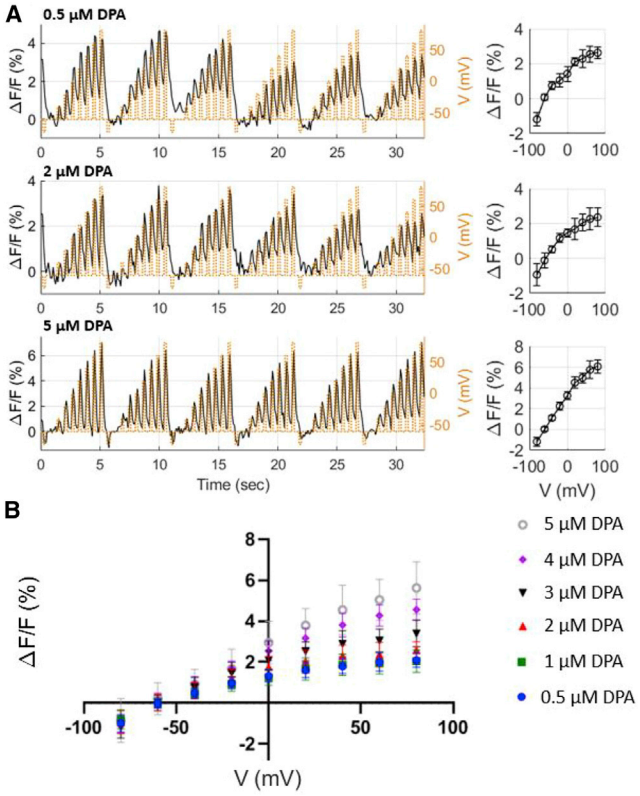

FIGURE 3 The fluorescence response of FPS beads/DPA in HEK cells for varying concentrations of DPA. (*A*) The fluorescence response of three cells in the presence of different concentrations of DPA are shown. The membrane potential was stepped in 20 mV increments from a holding potential of −60 mV. Each voltage level was held for 200 ms, followed by a repolarization step to −60 mV for 400 ms. Each trace was composed of six sweeps. The averaged fluorescence response of these cells at each voltage relative to −60 mV are shown on the right. Error bars correspond to SD.(*B*) The averaged relative changes in fluorescence ΔF/F upon changes in membrane potentials in the presence of different concentrations of DPA. Cells were labeled with 0.5 nM beads, and the fluorescence response for each DPA concentration was tested on several cells (5 μM DPA, n = 6; 4 μM DPA, n = 6; 3 μM DPA, n = 7; 2 μM DPA, n = 9; 1 μM DPA, n = 5; and 0.5 μM DPA, n = 7). Error bars correspond to SD.

FRET between DPA and endogenous proteins. Voltage-clamp experiments were conducted in cells applied with 2 μM DPA, without the addition of beads (Fig. S2 *A*). The averaged $\Delta F/F$ per 120 mV was 0.14 ± 0.04% (n = 3), indicating that there is no significant contribution to the beads/DPA response. Cells labeled with 0.5 nM beads only, without the addition of DPA (Fig. S2 *B*), were also tested. The averaged $\Delta F/F$ per 120 mV was 0.34 ± 0.14% (n = 12), which is a much smaller response than that of beads/DPA pair. A possible explanation for this response may be a change in ionic concentration at the vicinity of the bead's fluorophores because of the change in membrane potential.

Kinetics of FPS beads/DPA fluorescence response to change in membrane potential

Earlier work reported a fluorescence time constant of ∼0.1 ms in DiO/DPA FRET pair in HEK cells (21), similar to the speed of DPA movement in other preparations (∼0.1 ms) (22,23). Another estimation of ∼0.5 ms was reported in FRET pairs composed of DPA and membrane-tethered fluorescent proteins (24,25).

To assess the temporal resolution of the FPS beads/DPA pair, the fluorescence response was measured in HEK cells polarized with a short pulse from −60 to 60 mV (Fig. 4). The change in FPS beads fluorescence upon change in membrane potential was shown to be not instantaneous. The response fall time, defined as the duration needed for the fluorescent emission to decay from 90 to 10% from its maximal intensity value once the pulsed polarization ends, was measured to be 670 ms for a 1-s pulse (Fig. 4 *A*). A fluorescence response to changes in membrane potential was clearly observed for a polarization pulse 10 ms in duration (Fig. 4 *B*). However, no response was observed for depolarization pulses shorter than 5 ms, whereas DPA/DiO FRET pair showed a clear response to sub-ms pulses (Fig. S3). Thus, the temporal response of FPS beads/DPA is slower than was reported for other DPA FRET pairs, indicating that the FPS beads/DPA FRET pair is not suitable for measurements of AP-like signals. Becuase DPA translocates on the submillisecond timescale, it is likely that the issue of slow response is related to the bead location on the membrane and its response to changes in membrane potential. In longer pulse durations, the system gets to a voltage-related steady state as for the distance between the bead and DPA, whereas in short durations (≤5 ms), it might not get to this state yet.

Fluorescence response to membrane potential from single FPS beads

A major advantage of using beads as voltage detectors over fluorescent dyes may be the potential of recording from single beads on the nano (subdiffraction) scale. Thus, our next goal was to test the FPS beads/DPA FRET mechanism in single beads imaging. Isolated HEK cells were labeled with 1 or 5 pM FPS beads to achieve sparse staining (Fig. 5 *A*). Cells that were labeled with one to six single fluorescent spots after DPA application were chosen for the experiment. The 60 mV steps voltage-clamp protocol as described in Fig. 2 *C* was applied, and single regions of interest (ROIs) were detected for analysis (Fig. 5 *B*). Further description of spot detection analysis is described in Materials and methods. Representative fluorescence trajectories of single spots and their average are shown

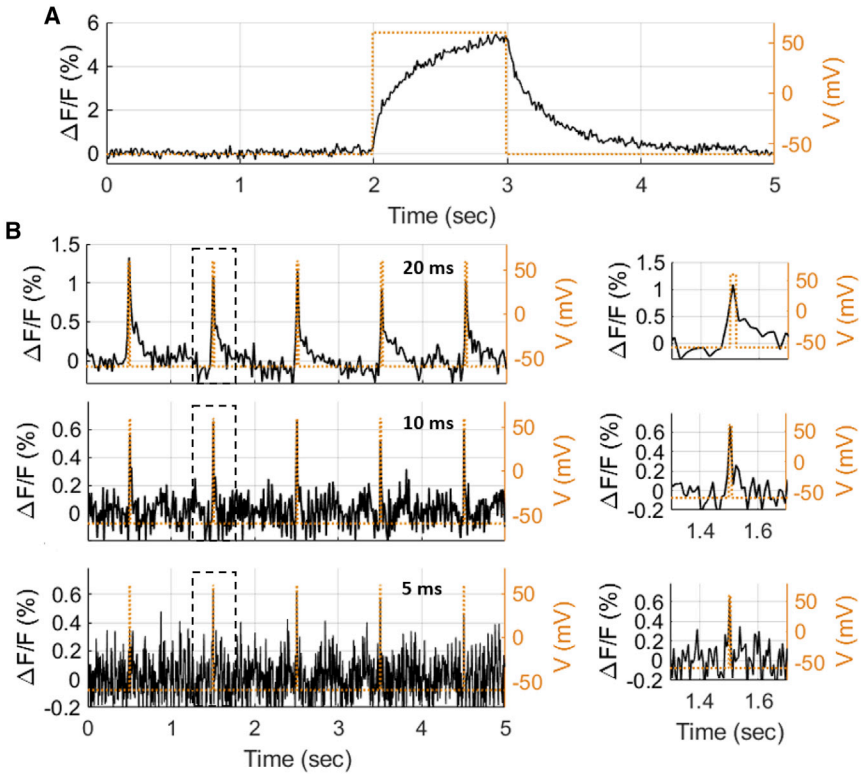

FIGURE 4 Response kinetics of FPS beads/DPA FRET pair to changes of membrane voltage in HEK cells. HEK cells were labeled with FPS beads, and voltage-clamp experiments were conducted in the presence of 2 μM DPA. The membrane potential was stepped from a holding potential of -60 to $+60$ mV at different pulse durations and repolarized back to -60 mV. (*A*) The change in fluorescence emission to 1-s pulse and imaging at a frame rate of 100 Hz. Slow response is observed at both the rising and falling parts of the polarization pulse. (*B*) The changes in fluorescence for 20-, 10-, and 5-ms pulses and imaging at a frame rate of 50, 100, and 200 Hz, respectively.

in Fig. 5, *C* and *D*, respectively. Only single spots that showed values larger than 2% for $\Delta F/F$ per 120 mV were ascribed as responsive spots. In the presence of 2 μM DPA, 21 single spots out of 27 were responsive (77.8%) and showed an averaged $\Delta F/F$ of 3.48 $\pm$ 1.02% (measured from eight cells). The presence of 5 μM DPA in the bath solution resulted in 12 responsive single spots out of 20 (60.0%) and showed a similar averaged $\Delta F/F$ of 3.33 $\pm$ 1.03% (measured from five cells) (Fig. 5 *E*). We note that the response for different beads was found to be heterogeneous. Fig. S4 shows the averaged optical response to changes in membrane potential calculated for each pixel in the imaged area for four individual HEK cells sparsely labeled with FPS beads. This variable response may occur from the heterogeneity of the beads, from the variability in the mode of interaction and proximity between the beads, cell membrane, and the surrounding DPA molecules and, to a lesser extent, because of local differences in membrane potential occurring in whole-cell patch clamping of cells.

Because the responsiveness of single spots in HEK cells was demonstrated, the fluorescence response of the FPS beads/DPA FRET pair to membrane potential was next examined in cultured neurons. DPA is a lipophilic anion; thus, it may affect excitable membranes by increasing their capacitance and changing their electrical response properties (22,25,26). This perturbation has been well documented in various systems in the presence of low micromolar concentrations of DPA. Previous reports have shown that this perturbation can be tolerated. It was found that DPA concentrations up to 5 μM led to no significant differences in action potential (AP) amplitude or spike threshold (22,25,27). To ensure the DPA concentration used in our experiments is suitable for cultured cortical neurons, whole-cell current clamp recordings were conducted in the presence of 1 and 2 μM and no DPA in the bath solution (Fig. 6). APs were evoked by depolarizing current pulses in 50 pA increments (100–250 pA, 300 ms); no APs were evoked after 50 pA depolarizing currents. For consistency, experiments testing different DPA concentrations were conducted at the same DIV. As shown in Fig. 6, *C–E*, these DPA concentrations had no significant effect on the first AP height, APs half-width, or threshold ($p > 0.05$).

The fluorescence response of FPS beads in neurons was tested in the presence of 2 μM DPA, the same concentration used in HEK cells, which was already proven to be effective as a voltage detector in combination with beads. Neurons were sparsely labeled with beads (22 pM), and single spots located on the neuron's soma were detected and analyzed as described in Materials and methods (Fig. 7). Representative fluorescence trajectories of single spots and their average during application of a 20-mV steps protocol are shown in Fig. 7, *C*

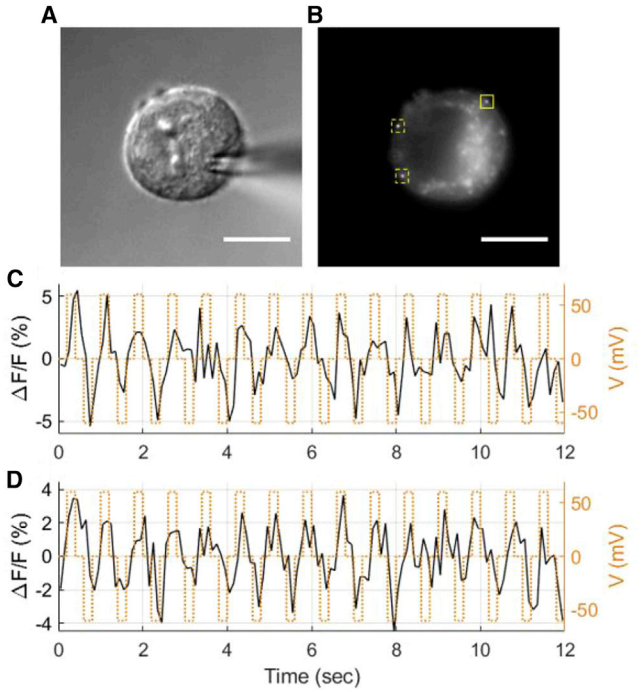

FIGURE 5 Optical responses to voltage of FPS beads/DPA FRET pair in HEK cells sparsely stained with beads. A DIC (*A*) and a fluorescence (*B*) image of a single HEK cell in the whole-cell patch-clamp mode, sparsely labeled with 5 pM beads, in the presence of 2 μM DPA in the bath solution. The voltage protocol is as described in Fig. 2 *C*. (*C*) and (*D*) show the fluorescence emission trajectory of one spot (indicated by the *solid yellow square*) and the averaged trajectory of three regions (indicated by *yellow squares*), respectively. The average relative change in fluorescence emission $\Delta F/F$ for the single spot and averaged trajectories was 4.5 $\pm$ 2.6% and 4 $\pm$ 1.4% per 120 mV, respectively. (*E*) The averaged change in fluorescence emission $\Delta F/F$ per 120 mV, measured from single ROIs in cells in the presence of 2 or 5 μM DPA in the bath solution. The cells were labeled with 1 or 5 pM beads, with the average performed over multiple ROIs in several cells (2 μM DPA, n = 21 measured from eight cells and 5 μM DPA, n = 12 measured from five cells). Error bars correspond to SD. Scale bars, 10 μm.

and *D*, respectively. The averaged $\Delta F/F$ per 100 mV, measured for 18 single spots in five cells, was 2.5 $\pm$ 1.0. Thus, the principle of using FPS beads and DPA as a FRET pair is successfully applicable for apparently single beads in neurons.

DISCUSSION

A new two-component system based on FRET between FPS beads as the fluorescent donors and DPA, a liphophilic anion that translocates between the leaflets of

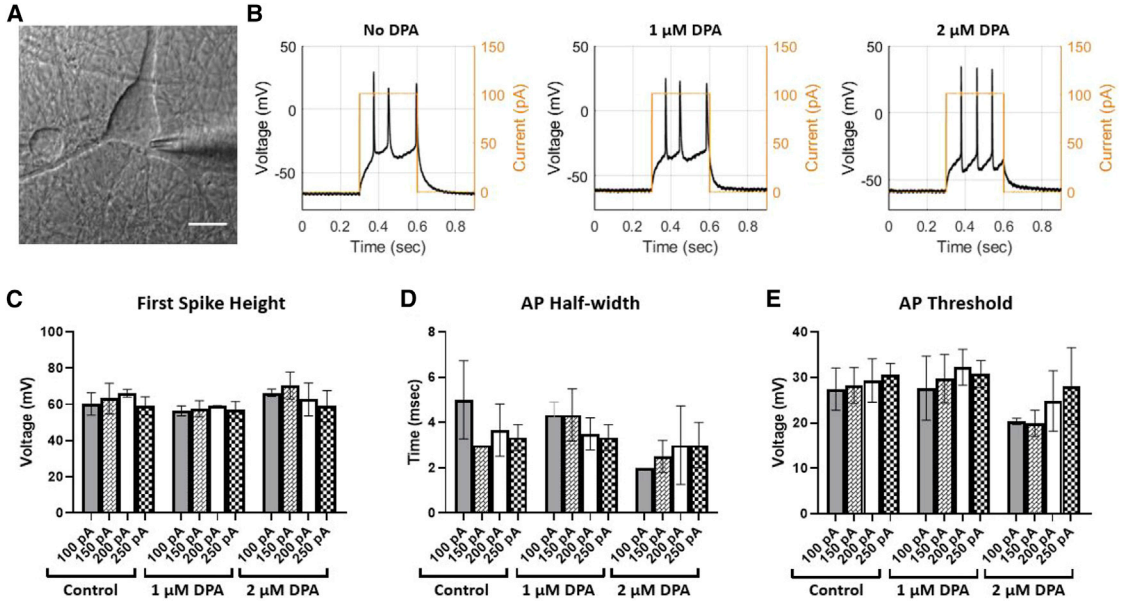

FIGURE 6 Electrical activity of cultured cortical neurons in the presence of different DPA concentrations. APs were recorded using the whole-cell configuration under the current clamp mode and were evoked by current injections. (*A*) A DIC image of a neuron in the whole-cell patch-clamp mode, showing the patch electrode. (*B*) Spiking activity evoked by a square depolarization current pulse of 150 pA for 300 ms. The traces are attributed to neurons without DPA in the bath solution (*left*) and in the presence of 1 μM DPA (*middle*) and 2 μM DPA (*right*). (*C–E*) Properties of the APs evoked by the protocol described in (*B*). APs properties were compared at different DPA concentrations and different amplitudes of depolarization current pulses. No significant difference was observed among columns and within columns (n = 3 for each treatment; $p > 0.05$; one-way-ANOVA).

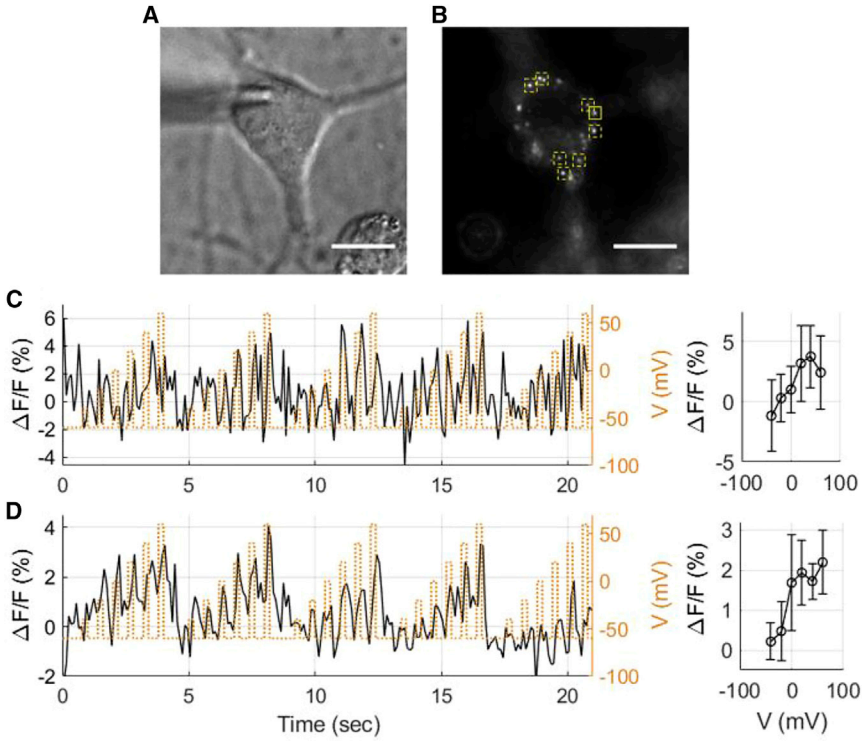

FIGURE 7 Optical responses to voltage of beads/DPA FRET pair in neurons sparsely stained with FPS beads. A DIC (*A*) and a fluorescence (*B*) image of a primary cortical neuron in the whole-cell patch-clamp mode, sparsely labeled with 22 pM beads, in the presence of 2 μM DPA in the bath solution. The membrane potential was stepped in 20 mV increments from a holding potential of −60 mV. Each voltage level was held for 200 ms, followed by a 400 ms repolarization step at −60 mV. Each trace was composed of five sweeps. (*C*) and (*D*) show the fluorescence emission trajectory (*left*) and average response (*right*) of one spot (indicated by the *solid yellow square*) and the average of nine spots (indicated by *yellow squares*), respectively. The average change in fluorescence emission ΔF/F for (*C*) and (*D*) was 3.2 ± 2% and 2.2 ± 1.3% per 100 mV, respectively. Error bars correspond to SD. Scale bars, 10 μm.

the membrane according to the membrane potential, is reported in this work (Fig. 1). This system is demonstrated to correlate the membrane potential with fluorescent intensity in HEK cells and cultured neurons over a range of applied voltages. The correlation was confirmed not only for ensemble staining but, more importantly, for single FPS beads.

This method has many required qualities over other approaches. First, the beads are applied to the extracellular solution and adsorbed to the cell membranes spontaneously over a few minutes with no apparent cytotoxicity. The commercial carboxyl-functionalized FPS beads used in this work are hydrophilic and negatively charged. Hence, no surface functionalization steps were needed for the adsorption of the beads to the cellular membranes. We note that the interaction of the beads with the membrane is not fully understood yet, and further characterization is needed. The FPS beads demonstrate high photostability and brightness, which allows visualization and recordings from single particles. As for DPA, it has attractive properties as an acceptor, such as rapid kinetics ($\tau < 0.5$ ms), high voltage sensitivity within the physiological range, good aqueous solubility, and low phototoxicity (21–23,26). However, because DPA increases the membrane capacitance, care must be taken to ensure work with concentrations that do not disrupt the native physiological responses (21). The DPA concentration used for this work was tested for the potential effect on the electrical properties of the neurons, and no significant effect was shown for 2 μM DPA, as was also reported by Bradley et al. (21). Altogether, in addition to the fact that the beads are commercially available in different sizes and can be synthesized with functional surface groups, they constitute an easy approach for single-particle voltage detection. FPS beads can further be targeted to specific proteins via conjugation of recognition molecules, thus targeted to specific cell types or subcompartments. Future work includes the conjugation of FPS beads to antibodies targeted to the extracellular domain of selected membrane proteins in cortical neurons. Considerations must be taken in choosing the right domain to minimize a potential interruption to the protein's function.

Measurements of APs demand a voltage sensor displaying a fast submillisecond temporal response. When DPA is used with small organic donor dyes (21,28–30), the temporal response of the FRET-based system is adequate to capture APs (31). However, the temporal response of FPS beads/DPA is estimated to be on the order of ∼5 ms(Fig. 4). This response is not suitable for capturing and recording APs. A similar slow temporal response was also observed with fluorescently labeled nanodisks acting as the donor construct (32). The observation of slow temporal response for two different types of nanoparticles points toward a similar underlying mechanism related to membrane adsorption. The reason for this slow

temporal response is the subject of future studies. Because DPA has rapid kinetics and DiO/DPA FRET pair shows a fast submillisecond response (21,24,25,33,34), it can be assumed that the speed limit is attributed to the FPS beads. One possible hypothesis is that the temporal response of FPS beads/DPA could be improved by anchoring the beads to the membrane through cross-linking to several membrane proteins or by decorating the bead's surface with long alkyl chains that can intercalate into the membrane. These approaches would be further investigated to maximize the FPS beads/DPA response in terms of kinetics.

In summary, we demonstrated the use of FPS beads as a nanoscale optical probe for membrane potential via FRET to voltage-dependent DPA. The necessity of an optical tool for detecting membrane potential changes in the single-molecule level is undisputed. Such a tool will enable the investigation of local membrane potential changes and may contribute dramatically to the understanding of biological processes in neuroscience. It can shed light on the interactions between different parts of a neuron as well as the interactions between neurons in a neural network. Here, we used a new and accessible platform for membrane potential imaging from single particles, which holds the possibility of targeting specific desired membrane proteins.

SUPPORTING MATERIAL

Supporting material can be found online at https://doi.org/10.1016/j.bpr.2021.100030.

DECLARATION OF INTERESTS

The authors declare no competing interests.

ACKNOWLEDGMENTS

This work has received funding from the European Research Council under the European Union's Horizon 2020 research and innovation program under grant agreement 669941, by the Human Frontier Science Program research grant RGP0061/2015, by the Biological and Environmental Research funding program of the Department of Energy Office of Science grant DE-FC03-02ER63421, by the STROBE National Science Foundation Science and Technology Center grant DMR-1548924, by the Israel Science Foundation grant 813/19, and by the Bar-Ilan Research and Development, the Israel Innovation Authority grant 63392.

REFERENCES

1. Salzberg, B. M., A. Grinvald, …, W. N. Ross. 1977. Optical recording of neuronal activity in an invertebrate central nervous system: simultaneous monitoring of several neurons. *J. Neurophysiol.* 40:1281–1291.
2. Deal, P. E., P. Liu, …, E. W. Miller. 2020. Covalently tethered rhodamine voltage reporters for high speed functional imaging in brain tissue. *J. Am. Chem. Soc.* 142:614–622.
3. Huang, Y. L., A. S. Walker, and E. W. Miller. 2015. A photostable silicon rhodamine platform for optical voltage sensing. *J. Am. Chem. Soc.* 137:10767–10776.
4. Yang, H. H., and F. St-Pierre. 2016. Genetically encoded voltage indicators: opportunities and challenges. *J. Neurosci.* 36:9977–9989.
5. Sjulson, L., and G. Miesenböck. 2007. Optical recording of action potentials and other discrete physiological events: a perspective from signal detection theory. *Physiology (Bethesda).* 22:47–55.
6. Baker, B. J., H. Lee, …, E. K. Kosmidis. 2007. Three fluorescent protein voltage sensors exhibit low plasma membrane expression in mammalian cells. *J. Neurosci. Methods.* 161:32–38.
7. Tsutsui, H., S. Karasawa, …, A. Miyawaki. 2008. Improving membrane voltage measurements using FRET with new fluorescent proteins. *Nat. Methods.* 5:683–685.
8. Kulkarni, R. U., and E. W. Miller. 2017. Voltage imaging: pitfalls and potential. *Biochemistry.* 56:5171–5177.
9. Adam, Y., J. J. Kim, …, A. E. Cohen. 2019. Voltage imaging and optogenetics reveal behaviour-dependent changes in hippocampal dynamics. *Nature.* 569:413–417.
10. Chien, M. P., D. Brinks, …, A. E. Cohen. 2021. Photoactivated voltage imaging in tissue with an archaerhodopsin-derived reporter. *Sci. Adv.* 7:eabe3216.
11. Piatkevich, K. D., S. Bensussen, …, X. Han. 2019. Population imaging of neural activity in awake behaving mice. *Nature.* 574:413–417.
12. Grenier, V., B. R. Daws, …, E. W. Miller. 2019. Spying on neuronal membrane potential with genetically targetable voltage indicators. *J. Am. Chem. Soc.* 141:1349–1358.
13. Park, K., Z. Deutsch, …, S. Weiss. 2012. Single molecule quantum-confined Stark effect measurements of semiconductor nanoparticles at room temperature. *ACS Nano.* 6:10013–10023.
14. Derfus, A. M., W. C. W. Chan, and S. N. Bhatia. 2004. Probing the cytotoxicity of semiconductor quantum dots. *Nano Lett.* 4:11–18.
15. Ipe, B. I., M. Lehnig, and C. M. Niemeyer. 2005. On the generation of free radical species from quantum dots. *Small.* 1:706–709.
16. Hoshino, A., K. Fujioka, …, K. Yamamto. 2004. Physicochemical properties and cellular toxicity of nanocrystal quantum dots depend on their surface modification. *Nano Lett.* 4:2163–2169.
17. Bakalova, R., H. Ohba, …, Y. Baba. 2004. Quantum dot anti-CD conjugates: are they potential photosensitizers or potentiators of classical photosensitizing agents in photodynamic therapy of cancer? *Nano Lett.* 4:1567–1573.
18. Ibrahim, S. A., W. Ahmed, and T. Youssef. 2015. Role of ZnS shell on stability, cytotoxicity, and photocytotoxicity of water-soluble CdSe semiconductor quantum dots surface modified with glutathione. *J. Nanophotonics.* 9:093090.
19. González, J. E., and R. Y. Tsien. 1995. Voltage sensing by fluorescence resonance energy transfer in single cells. *Biophys. J.* 69:1272–1280.
20. Jayant, K., J. J. Hirtz, …, R. Yuste. 2017. Targeted intracellular voltage recordings from dendritic spines using quantum-dot-coated nanopipettes. *Nat. Nanotechnol.* 12:335–342.
21. Bradley, J., R. Luo, …, D. A. DiGregorio. 2009. Submillisecond optical reporting of membrane potential in situ using a neuronal tracer dye. *J. Neurosci.* 29:9197–9209.
22. Fernández, J. M., R. E. Taylor, and F. Bezanilla. 1983. Induced capacitance in the squid giant axon. Lipophilic ion displacement currents. *J. Gen. Physiol.* 82:331–346.
23. Lu, C. C., A. Kabakov, …, D. W. Hilgemann. 1995. Membrane transport mechanisms probed by capacitance measurements

with megahertz voltage clamp. *Proc. Natl. Acad. Sci. USA.* 92:11220–11224.

24. Chanda, B., R. Blunck, …, F. Bezanilla. 2005. A hybrid approach to measuring electrical activity in genetically specified neurons. *Nat. Neurosci.* 8:1619–1626.
25. DiFranco, M., J. Capote, …, J. L. Vergara. 2007. Voltage-dependent dynamic FRET signals from the transverse tubules in mammalian skeletal muscle fibers. *J. Gen. Physiol.* 130:581–600.
26. Chanda, B., O. K. Asamoah, …, F. Bezanilla. 2005. Gating charge displacement in voltage-gated ion channels involves limited transmembrane movement. *Nature.* 436:852–856.
27. Oberhauser, A. F., and J. M. Fernandez. 1995. Hydrophobic ions amplify the capacitive currents used to measure exocytotic fusion. *Biophys. J.* 69:451–459.
28. Salzberg, B. M., A. L. Obaid, and F. Bezanilla. 1993. Microsecond response of a voltage-sensitive merocyanine dye: fast voltage-clamp measurements on squid giant axon. *Jpn. J. Physiol.* 43 (*Suppl 1*):S37–S41.
29. Rohr, S., and B. M. Salzberg. 1994. Multiple site optical recording of transmembrane voltage (MSORTV) in patterned growth heart cell cultures: assessing electrical behavior, with microsecond resolution, on a cellular and subcellular scale. *Biophys. J.* 67:1301–1315.
30. Fink, A. E., K. J. Bender, …, D. A. DiGregorio. 2012. Two-photon compatibility and single-voxel, single-trial detection of subthreshold neuronal activity by a two-component optical voltage sensor. *PLoS One.* 7:e41434.
31. Wang, W., C. K. Kim, and A. Y. Ting. 2019. Molecular tools for imaging and recording neuronal activity. *Nat. Chem. Biol.* 15:101–110.
32. Grupi, A., Z. Shapira, …, S. Weiss. 2021. Point-localized, site-specific membrane potential optical recording by single fluorescent nanodiscs. *Biophys. Rep.* 1.
33. Hamill, O. P., A. Marty, …, F. J. Sigworth. 1981. Improved patch-clamp techniques for high-resolution current recording from cells and cell-free membrane patches. *Pflugers Arch.* 391:85–100.
34. Alivisatos, A. P., M. Chun, …, R. Yuste. 2012. The brain activity map project and the challenge of functional connectomics. *Neuron.* 74:970–974.